DFT and TD-DFT Calculations on the Electronic Structures and Spectroscopic Properties of Cyclometalated Platinum(II) Complexes

Xin Zhou,[†] Qing-Jiang Pan,[‡] Bao-Hui Xia,[§] Ming-Xia Li,[†,‡] Hong-Xing Zhang,*[,†] and Au-Chin Tung[†]

State Key Laboratory of Theoretical and Computational Chemistry, Institute of Theoretical Chemistry, and College of Chemistry, Jilin University, Changchun 130023, People's Republic of China, and School of Chemistry and Materials Science, Heilongjiang University, Haerbin 150080, People's Republic of China

Received: June 28, 2006; In Final Form: April 13, 2007

The electronic structures and spectroscopic properties of the three tridentate cyclometalated Pt(II) complexes Pt(N^N^C)C≡CPh (N^N^CH = 6-phenyl-2,2′-bipyridine) (**1**), Pt(N^N^S)C≡CPh (N^N^SH = 6-thienyl-2,2′-bipyridine) (**2**), and Pt(N^N^O)C≡CPh (N^N^OH = 6-furyl-2,2′-bipyridine) (**3**) were investigated theoretically using the density functional theory (DFT) method. The geometric structures of the complexes in the ground and excited states were explored at the B3LYP and UB3LYP levels, respectively. The absorption and emission spectra of the complexes in CH_2Cl_2 and CH_3CN solutions were calculated by time-dependent density functional theory (TD-DFT) with the PCM solvent model. The calculated energies of the lowest singlet state and lowest triplet state in the three complexes are in good agreement with the results of experimental absorption and luminescence studies. All of the lowest-lying transitions were categorized as LLCT combined with MLCT transitions. The 623-nm emission of **1** from the $^3A' \rightarrow {}^1A'$ transition was assigned as ^{3}LLCT and ^{3}MLCT transitions, whereas the 657- and 681-nm emissions of **2** and **3**, respectively, were attributed to ^{3}ILCT perturbed by ^{3}MLCT transitions. NLO response calculations revealed that the nonzero values of the static first hyperpolarizability (β_0) for **1**−**3** are greatly enhanced through the introduction of the metal Pt(II) into the cyclometalated ligands, an effect that is determined by MLCT and LLCT transitions.

1. Introduction

Research on the photophysics and photochemistry of polypyridyl platinum(II) complexes continues to be of interest in the chemical community. One key reason for this interest is that platinum(II) complexes can exhibit a variety of charge-transfer (CT) excited states,[1] such as MLCT (metal-to-ligand charge transfer), LLCT (ligand-to-ligand charge transfer), and ILCT (intraligand charge transfer, $\pi\pi^*$). The directional nature of the CT excited states in square-planar platinum(II) complexes is ideal for electron−hole creation and separation,[2] and consequently, these systems merit consideration for use in molecular photochemical devices and related supramolecular systems. On the other hand, the unique axial interactions existing in square-planar polypyridyl platinum(II) complexes can give rise to the possibility for types of interactions that are not possible in octahedral and tetrahedral metal complexes. For example, excimer formation and excimer emission have been observed in some instances when face-to-face complex formation promotes delocalization of the excitation through metal−metal interactions.[3] In addition, polypyridyl platinum(II) complexes also can interact with biological macromolecules such as DNA as anticancer agents.[4]

To this day, long-lived emission and high luminescent efficiency are the long-term goals pursued for luminescent polypyridyl platinum(II) complexes. However, many platinum(II) complexes with simple polypyridy ligands, such as [Pt(trpy)Cl]$^+$ (trpy = 2,2′,6′,2″-terpyridine), are scarcely emissive at room temperature.[5] This is because the decay originates from the efficient nonradiative d−d state, which is lower in energy than radiative CT excited states. Therefore, switching of the energy order between the nonradiative d−d and radiative CT excited states for [Pt(trpy)Cl]$^+$ is vital to obtain effective and long-lasting emissions. In general, for transition metal complexes that exhibit CT transitions, the electronic structure of the ligand plays a crucial role in determining the photophysical properties of the complexes. The reason is that the ligands influence either the basicity of the donor or the energies of the unoccupied orbitals and, therefore, have an impact on the excited-state properties of molecules. In the past decade, many studies have reported methods for changing the energy order between the d−d and CT states for terpyridyl Pt(II) complexes, and two classic strategies have emerged: (1) The weak-field ligand can be replaced by a strong-field ligand, as in the replacement of Cl anion by strong-field acetylide derivates reported by Yam et al.,[6] which effectively destabilizes the filled platinum d levels relative to the terpyridine π and π^* levels and thus places the ^{3}MLCT excited state below the ^{3}d−d state. (2) An aryl group can be introduced into the 4′-coordinated position of the terpyrdine ligand,[7] because the extended π-coordinated conjugation between the aryl substituent and terpyridine ligand significantly lowers the energy of the π^*-based LUMO, so that the lowest ^{3}LLCT excited state lies at a lower energy than the ^{3}d−d state. By use of these two strategies, many long-lifetime luminescent emitters have been synthesized.[6,7] In addition, another effective means of adjusting the energy order is replacing the terpyridyl ligand by a cyclometalating analogue

* To whom correspondence should be addressed. E-mail: zhanghx@mail.jlu.edu.cn.
† State Key Laboratory of Theoretical and Computational Chemistry, Institute of Theoretical Chemistry, Jilin University.
‡ Heilongjiang University.
§ College of Chemistry, Jilin University.

10.1021/jp064044r CCC: $37.00 © 2007 American Chemical Society
Published on Web 06/05/2007

because the strong field induced by the cyclometalated carbon can also serve to raise the energy of the deactivating d−d states. This approach has led to a variety of emissive complexes, including several containing N^C^N and N^N^C ligands.[8]

Very recently, a series of N^N^A-coordinated (N^N^AH = 6-aryl-2,2′-bipyridine) platinum(II) complexes were synthesized and structurally characterized.[9] These complexes exhibit superior emissive properties and higher quantum yields than the 2,2′:6′,2″-terpyridine (trpy) congeners (almost 1 order of magnitude). Moreover, the modifications of the tridentate ligands in these complexes can result in subtle tuning of their structural, photophysical, and luminescent characteristics and provide a novel family of electrophosphorescent emitters. For example, through the replacement of N^N^C (N^N^CH = 6-phenyl-2,2′-bipyridine) by N^N^S (N^N^SH = 6-thienyl-2,2′-coordinated bipyridine) and N^N^O (N^N^OH = 6-furyl-2,2′-bipyridine), two distinct types of emission behaviors have emerged among the cyclometalated platinum(II) complexes, i.e., N^N^C-coordinated complexes exhibit yellow light emissions, whereas N^N^S- and N^N^O-coordinated complexes emit orange-red and saturated light. In addition to being applied in luminescent materials, cyclometalated platinum(II) complexes containing arylacetylide ligand can also serve as potential nonlinear optical (NLO) materials. Because a CT excited state can produce electrons and holes and make it possible for the electrons and holes to interact, this is a fundamental characteristic of NLO materials. NLO responses of terpyridyl transition metal (Ru, Zn, and Ir)[10] complexes have been observed, and it was suggested that the nature of the CT excited state is strongly related to the NLO response.

Although differences in the luminescence properties of the N^N^A-coordinated platinum(II) complexes have been observed, no intrinsic reason for these differences was proposed. The correct description of the electronic transitions in cyclometaltated platinum(II) complexes is much needed, not only because of the importance of CT excited states but also because of the importance of understanding the dramatic dependence of the photophysics and photochemistry of these complexes on the tridentate ligands. Therefore, a detailed theoretical investigation of the electronic transitions of the complexes Pt(N^N^C)C≡CPh (**1**), Pt(N^N^S)C≡CPh (**2**), and Pt(N^N^O)C≡CPh (**3**) was undertaken using density functional (DF) techniques. The study was carried out with several goals: (1) to make a complete assignment of the UV/vis spectra of **1**−**3** with a special emphasis on the low-energy transitions responsible for the visible absorption, (2) to establish the electronic structures of **1**−**3** and understand their different emission behaviors, and (3) to explore the potential use of these complexes in NLO materials.

2. Computational Details and Theory

The geometric structures of **1**−**3** in the ground state (S_0) and lowest-energy triplet state (T_1) were fully optimized at the B3LYP[11] and unrestricted B3LYP (UB3LYP) levels, respectively. The ground- and excited-state calculations were symmetry-restricted to C_s point group. Using the respective optimized S_0 and T_1 geometries of **1**−**3**, we employed time-dependent density functional theory (TD-DFT)[12] at the B3LYP level to predict their absorptions and emissions. Considering the differences of the absorption and emission behaviors in gas and solution, the solvent effects of CH_2Cl_2 and CH_3CN were taken into account by means of the polarizable continuum model (PCM).[13]

Because the different aromaticities in the phenyl, thienyl, and furyl rings can lead to different electronic structures and spectroscopic properties, the aromaticities of the aryl rings should be taken into account. Here, the nucleus-independent chemical shift (NICS)[14] values were used as an aromaticity index to evaluate the aromaticity of the systems. NICS values provide an "absolute" measure of cyclic conjugated π-electron systems and are computed at selected points inside or around molecules (typically at the ring center or the r_a distance above it). This approach is noted for not requiring reference molecules and increment schemes. Thus, in this work, to better analyze the aromaticities of the cyclic electron delocalization systems, we chose NICS(1) (at the point of $r_a = 1$ Å) as the aromaticity index to describe the aromaticities of the aryl rings. (The particulars are detailed in the following sections.)

Furthermore, the NLO properties for **1**−**3** were estimated at the DFT level, with the dipole moment (μ), polarizability (α), and static first hyperpolarizability (β_0) defined by the following formulas[15]

$$\mu = (\mu_x^2 + \mu_y^2 + \mu_z^2)^{1/2} \quad (1)$$

$$\alpha = \frac{1}{3}(\alpha_{xx} + \alpha_{yy} + \alpha_{zz}) \quad (2)$$

$$\beta_0 = (\beta_x^2 + \beta_y^2 + \beta_z^2)^{1/2} \quad (3)$$

All calculations were performed using the Gaussian 03 program.[16] The LANL2DZ and 6-31G(d) basis sets were employed for the Pt(II) atom and for the other atoms, respectively. To better explore the NLO responses of **1**−**3**, the 6-311G-(d,p) basis set was employed for the nonmetal atoms in the NLO calculations. In addition, one f-type polarization function ($\alpha_f = 0.14$)[17] was augmented to the Pt(II) atom. It has been shown that such a polarization function on a heavy atom is necessary to obtain reasonable geometric structures and accurate spectroscopic properties.[18]

3. Results and Discussions

3.1. Geometric Structures in the S_0 and T_1 States. The optimized S_0 structures of **1**−**3**, along with the coordination axis, are depicted in Figure 1, and the corresponding important parameters are listed in Table 1. The only difference between **1**−**3** and the well-studied $[Pt(trpy)C{\equiv}CPh]^+$ is the replacement of one lateral pyridine in terpyridine by a phenyl, thienyl, and furyl, respectively. The replacement does not have an impact on the geometric structure of **1**−**3**, and similarities in the bond lengths and angles to the analogous complex $[Pt(trpy)C{\equiv}CPh]^+$ are shown. As reported in Table 1, the geometrical parameters of **1**−**3** are comparable to the experimental values for Pt(N^N^C)C≡CPh.[9] The metal−ligand bond lengths fall into the range of the values measured in other polypyridine Pt(II) complexes. The calculated Pt−C and Pt−N bond lengths of 2.009 and 2.058 Å for **1** are 0.017 and 0.07 Å longer, respectively, than the experimentally observed values. The slight differences come from the crystal lattice distortion existing in the real molecules. For the three complexes, the coordination geometry of Pt(II) exhibits a quasi-square-planar conformation, evidenced by a deviation of the N1−Pt−N2 and N1−Pt−C1 bond angles by ca. 9−14° from 90°, which is expected for Pt(II) complexes and agrees well with the experimental values.

Upon excitation, the bond angles of **1**−**3** in the excited state are almost identical to those in the ground state, but there are some contrary trends in the bond lengths: (1) The Pt−C1 bond of **1** in the T_1 state is ca. 0.023 Å longer than that in the S_0 state, whereas those of **2** and **3** are 0.038 and 0.016 Å shorter,

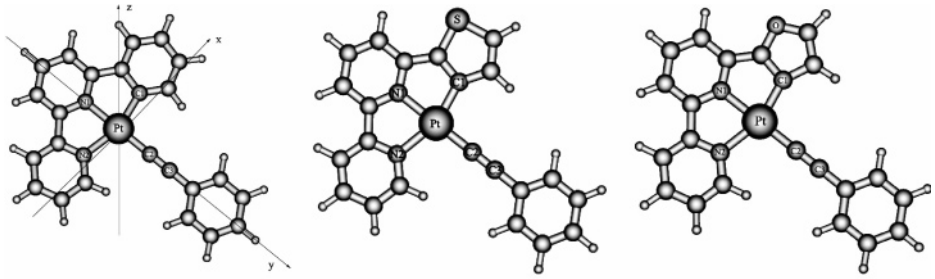

1 **2** **3**

Figure 1. DFT-optimized geometric structures of **1**−**3** in the ground state at the B3LYP level.

TABLE 1: Partial Optimized Geometric Structural Parameters of 1−3 in the Ground and Excited States Compared to the Experimental Values of 1 in the Ground State

	1			**2**		**3**	
	electronic state						
	^{1}A′	^{3}A′	exp[a]	^{1}A′	^{3}A′	^{1}A′	^{3}A′
	bond lengths (Å)						
Pt−N1	2.058	2.029	1.987	2.069	2.060	2.083	2.038
Pt−N2	2.128	2.113	2.123	2.124	2.096	2.125	2.092
Pt−C1	2.009	2.032	1.992	2.003	1.965	2.002	1.986
Pt−C2	1.960	1.908	1.970	1.959	1.955	1.956	1.955
C2≡C3	1.228	1.254	1.185	1.228	1.235	1.227	1.234
	bond angles (deg)						
N1−Pt−N2	77.1	77.3	78.4	77.0	77.0	76.7	77.1
N1−Pt−C1	81.0	81.4	82.1	80.5	81.5	80.4	81.5

[a] Reference 9.

respectively, than the corresponding values of the S_0 state. (2) The Pt−C2 bond length of **1** is shortened in the T_1 state, but no notable changes are found in **2** and **3**. (3) The C≡C triplet bond of **1** is elongated by about 0.03 Å, whereas the elongations of the C≡C bond for **2** and **3** are less than 0.01 Å. It is well-known that the bond interaction between metal and ligand can be described as a donation from a σ molecular orbital of the ligand toward an empty d orbital of the metal and a concurrent back-donation from a filled d orbital to a π^* antibonding orbital of the ligand. According to this statement, the Pt(II)−ligand bond lengths should be correlated with the number of d electrons of Pt(II) that are back-donated to the ligands. Therefore, it can be concluded that the characters of the CT transitions occurring in **1**−**3** must be different.

3.2. Aromaticity. Because only the lateral aryl rings are different for **1**−**3**, it is necessary to explore the aromaticity of the aryl ligands, which usually can influence the properties of the electronic structure and excited state. Because the phenyl, thienyl, and furyl ligands are all cyclic conjugated π-electron systems, we need to choose an appropriate aromaticity index. According to the conclusions of Schleyer et al.,[14] for cyclic conjugated π-electron systems, at points such that $r_a < 1$ Å, the NICS values cannot reveal the aromaticity of the π-conjugation systems accurately because σ-bonding character is dominant in this region. However, at points with $r_a > 1$ Å, although the π-bonding character is overwhelming relative to the σ-bonding character, the NICS values are increasingly "nonaromatic". Therefore, NICS(1) is the preferred index for describing the aromaticity of aryl rings in this work. The NICS(1) values of the phenyl, thienyl, and furyl ligands in **1**−**3** were calculated at the DFT level. The calculated NICS values of the phenyl, thienyl, and furyl ligands are plotted versus r_a (0.0−2.0 Å) in Figure S2 (Supporting Information). As seen in Figure S2, the turning point in the curve occurs around $r_a = 1$ Å, so NICS(1) is further demonstrated to be an appropriate index.

The DFT-calculated NICS(1) values of the phenyl, thienyl, and furyl ligands are −7.918, −7.473, and −7.436 ppm, respectively, so the aromaticities of the three aryl rings are in the order phenyl > thienyl > furyl. Because of the presence of the π-orbital interactions between the lateral aryl ligand and the central pyridyl ligand, the aromaticity of the central rings is much influenced. The dissected NICS(1) values of the N^N^C, N^N^S, and N^N^O rings in **1**−**3** are reported in Table S1. As shown in Table S1, the NICS(1) values of the central pyridyl ring of **1**−**3** are −6.664, −5.833, and −5.477 ppm, whereas those of the other lateral pyridyl ring are −8.718, −8.678, and −8.691 ppm, respectively. Obviously, the aromaticities of the central pyridyl rings of **1**−**3** are weaker than those of the lateral rings because the central rings have to share the π electrons with two neighbors. If the aromaticity of the cyclometalated ligand was simply assumed to be the summation of all of the fragmental aromaticities, the aromaticity values should be in the order N^N^C (−22.30 ppm) > N^N^S (−21.98 ppm) > N^N^O (−21.60 ppm).

3.3. Absorption Spectra. The absorption spectra in CH_2Cl_2 solution for **1**−**3** were explored using the PCM model in SCRF, in which the solvent is simulated as a continuum of uniform dielectric constant ϵ. To discuss the absorption behavior in detail, we first reveal the Kohn−Sham orbitals for **1**−**3** (Table 2). As seen in Table 2, because of the similar molecular structures, the Kohn−Sham orbitals exhibit considerable similarities in composition in **1**−**3**. On the basis of the data listed in Table 2, five conclusions can be drawn: (1) The HOMOs (highest occupied molecular orbitals) 16a″ (**1**), 17a″ (**2**), and 16a″ (**3**) are of $\pi^*\{d_{yz}(Pt)-\pi^*[\pi(C\equiv C)-\pi^*(Ph)]\}$ character coming from the combination of the Pt(II) d_{yz} orbital (30%) and the π^*(C≡CPh) orbital (64%), whereas the HOMO − 1 orbitals for **1**−**3** consist of the π^* orbital localized on the cyclometalated ligand and the Pt(II) d_{xz} orbital, although the composition of Pt(II) is about 20% higher for **1** than **2** and **3**. In addition, the

TABLE 2: Compositions of Frontier MOs in the Ground State for 1−3 in CH_2Cl_2 Solution

1

			N^N^C		
MO	*E* (eV)	Pt	bipyridine	phenyl	C≡CPh
81a′	0.3154	11.8p + 24.3$d_{x^2-y^2}$	40.8	12.7	9.2
23a″	0.2411	6.2p + 2.6d	19.5	56.3	15.3
22a″	0.1782				99.9
21a″	−0.0942		84.3	13.3	
20a″	−0.4006	7.8p + 3.1d_{yz}	10.5	4.6	73.9
19a″	−1.1655		94.8	2.8	
18a″	−1.6289		74.6	21.5	
17a″[a]	−2.2880	2.8p + 2.9d_{yz}	88.9	2.8	2.7
16a″[b]	−5.2641	29.7d_{yz}	5.2		63.1
15a″	−5.7169	44.0d_{xz}	19.2	36.4	
80a′	−5.7310	1.1p + 36.5d_{xy}	12.2	4.8	44.6
79a′	−6.1915	21.0s + 73.4d_{z^2}	1.5	2.1	
14a″	−6.4388	7.7d_{xz}	45.9	45.1	
13a″	−6.6772				100.0
12a″	−6.9681	48.9d_{yz}	19.1		31.9
11a″	−7.4016	8.5d_{xz}	65.6	20.5	5.4

2

			N^N^S		
MO	*E* (eV)	Pt	bipyridine	thienyl	C≡CPh
81a′	0.0857	5.8p + 20.9$d_{x^2-y^2}$	30.0	36.0	6.1
22a″	−0.1725		76.5	21.4	
21a″	−0.3799	5.9p + 3.5d_{yz}		3.4	81.2
20a″	−1.1715	0.5p + 2.0d_{xz}	93.1	3.9	
19a″	−1.6784		66.8	28.1	
18a″[a]	−2.3133	3.0p + 2.7d_{yz}	86.6	4.8	2.9
17a″[b]	−5.3065	29.1d_{yz}			63.9
16a″	−5.5490	29.7d_{xz}	22.4	47.7	
80a′	−5.7906	1.0p + 36.1d_{xy}	9.5	5.3	47.7
79a′	−6.2649	20.3s + 74.9d_{z^2}			
15a″	−6.4279	20.8d_{xz}	10.0	68.5	
14a″	−6.6916				100.0
13a″	−7.0113	47.4d_{yz}	21.0		31.5
12a″	−7.3733	7.1d_{yz}	72.3	14.3	6.3
11a″	−7.5518	47.0d_{xz}	16.1	36.4	

3

			N^N^O		
MO	*E* (eV)	Pt	bipyridine	furyl	C≡CPh
78a′	0.2220	9.3p + 27.9$d_{x^2-y^2}$	38.5	13.8	9.4
22a″	0.1671				100.0
21a″	−0.0389		85.8	11.5	
20a″	−0.3725	6.1p + 3.7d_{yz}			79.3
19a″	−1.1440		92.4		
18a″	−1.5701		75.3	19.2	1.8
17a″[a]	−2.2931	2.8p + 2.7d_{xz}	89.0		2.7
16a″[b]	−5.3046	1.0p + 29.4d_{yz}			64.1
15a″	−5.4314	25.1d_{xz}	25.1	49.3	
77a′	−5.7830	35.8d_{xy}	10.0	5.4	47.8
76a′	−6.2614	20.1s + 75.7d_{z^2}			
14a″	−6.6554	46.9d_{xz}	8.6	44.2	
13a″	−6.6881				100.0
12a″	−7.0154	47.1d_{yz}	21.2		31.6
11a″	−7.3515	7.8d_{yz}	75.7	10.2	6.4

[a] LUMO. [b] HOMO.

composition of the HOMO − 2 is analogous to that of the HOMO for **1**−**3**, in which the Pt d_{yx} orbital is replaced by the Pt d_{xy} orbital. (2) The HOMO − 3 of **1**−**3**, 0.93−0.95 eV lower than the HOMO, comes completely from the Pt(II) s + d_{z^2} atomic orbitals (>95%) and is a metal-based orbital in all considered Kohn−Sham orbitals. (3) The composition of the HOMO − 4 is similar to that of the HOMO − 1. The HOMO − 4 of **1** (14a″) at −6.44 eV is localized more than 91% on the N^N^C plane, whereas those of **2** (15a″) and **3** (14a″) are basically dominated by the metal Pt d orbital and the furyl or thienyl ligands with some bipyridine ligand. (4) With respect to the unoccupied Kohn−Sham orbitals for the three complexes, the LUMOs (lowest unoccupied molecular orbitals), about ca. 3.0 eV above the HOMOs, are composed of nearly 90% bipyridine ligand, whereas the LUMO + 1 contains contributions from the π^* orbital of N^N^C, N^N^S, and N^N^O, respectively. In addition, the LUMO + 2 and LUMO + 3 are mainly localized on the diimine and phenylacetylide ligands, respectively. (5) We observe that the virtual orbitals have larger contributions from the cyclometalated ligands, except for the LUMO + 7 of **1**, LUMO + 5 of **2**, and LUMO + 6 of **3** (which have 26−36% Pt contribution and 53−66% cyclometalated contribution), and the LUMO + 3 of **2** and the LUMO + 5 of **1** and **3** (which are almost exclusively located on the C≡CPh ligand). To intuitively understand the Kohn−Sham orbitals described above, the electronic density diagrams of which are presented in Figure 2, Table 3 gives the absorption data in terms of the transition states, excitation energies, excitations with maximum CI coefficients, and oscillator strengths for **1**−**3** in CH_2Cl_2 solution. For clarity, we list in Table 3 only the most leading excited states with the largest |CI coefficients|. As revealed in Table 3, the dipole-allowed lowest-lying absorptions from the $X^1A' \rightarrow A^1A'$ transition are at 505, 501, and 498 nm for **1**, **2**, and **3**, respectively, in which the leading excitation configuration of HOMO → LUMO is responsible for the transition. Table 3 shows that the HOMOs 16a″ (**1**), 17a″ (**2**), and 16a″ (**3**) are composed of ca. 30% metal Pt(II) and 64% C≡CPh ligand, whereas the LUMOs are mainly (about 90%) localized on the bipyridine fragments. Therefore, the lowest-lying absorptions are attributed to combined transitions of C≡CPh → bipyridine charge transfer (LLCT) and Pt(II) → bipyridine charge transfer (MLCT). Within the investigated UV/vis region, higher-energy absorption with the largest oscillator strength at λ < 300 nm occurs for **1**−**3**, and two major excitations of HOMO − 4 → LUMO + 1 and HOMO → LUMO + 3 contribute to the absorption. We can see from Figure 2 that the HOMO − 4 is localized on the cyclometalated ligand and the LUMO + 1 comes from the Pt atom and the C≡CPh ligand. Thus, the higher-energy absorptions are assigned to an ILCT transition and combined with an MLCT transition. The rest of the calculated absorptions can be seen in Table 3. The calculated absorption spectra of **1**−**3** are simulated by a Gaussian-type curve in Figure 3a, and the experimentally measured absorption spectra in CH_2Cl_2 solution at room temperature for **1**−**3** are shown in Figure 3b. From Figure 3, one can see that the experimental spectra of **1**−**3** are well reproduced by the present calculations but with some red shifts in wavelength for the low-lying MLCT/LLCT absorption band (ca. 0.2−0.3 eV). The moderate shift can be ascribed to the deficiency of the flexibility in the TD-DFT method in describing states with significant charge transfer.

The d−d state is usually regarded as the intrinsic reason for the nonemission of square-planar Pt(II) complexes in solution. Therefore, stabilizing and deactivating the d−d excited state is of great significance in experiments. In the calculations, the energy gap of the d−d state was found to be 6.51, 6.35, and 6.48 eV for **1**, **2**, and **3**, respectively, which is much greater than those of MLCT, LLCT, and ILCT transitions (Table 3). As a result, in competition with the CT transitions, the d−d excited state is unavailable.

It is worth noting that differences in solvent polarity will dramatically influence the MO energies in different solutions and, hence, change the absorption energies. Therefore, to

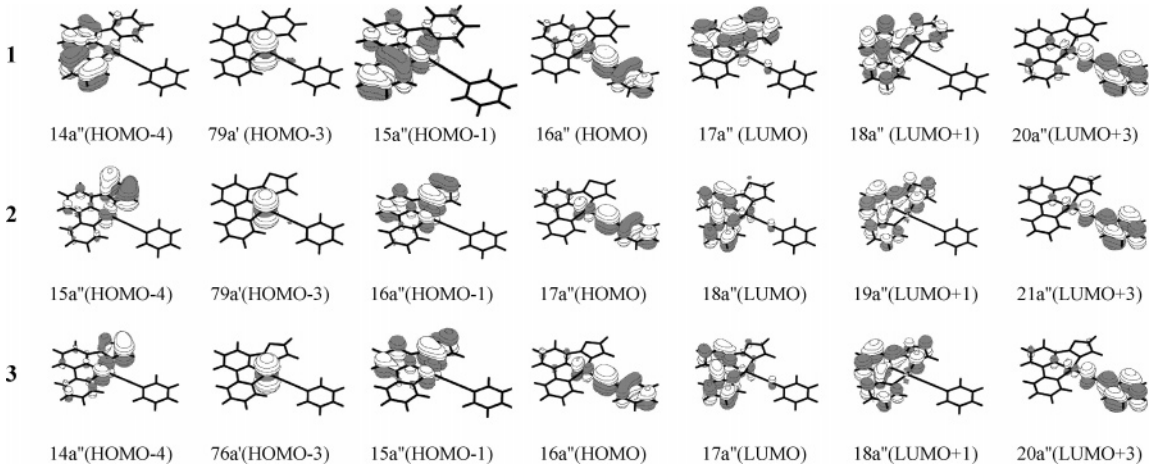

Figure 2. Electronic density diagrams of partial MOs of **1**−**3**.

TABLE 3: Absorptions of 1−3 in CH_2Cl_2 Solution According to TD-DFT (B3LYP) Calculations

transition	excitation	coeff	*E* (eV) (nm)	oscillator	assignment
		1			
$X^1A' \rightarrow A^1A'$	16a″ → 17a″	0.68	2.46 (505)	0.1577	MLCT/LLCT
$X^1A'' \rightarrow B^1A''$	79a′ → 17a″	0.70	3.01 (412)	0.0038	MLCT
$X^1A' \rightarrow C^1A'$	16a″ → 18a″	0.69	3.10 (401)	0.0721	MLCT/LLCT
$X^1A' \rightarrow D^1A'$	14a″ → 17a″	0.67	3.60 (344)	0.1430	MLCT/LLCT
$X^1A' \rightarrow E^1A'$	14a″ → 18a″	0.55	4.32 (287)	0.3171	MLCT/ILCT
$X^1A' \rightarrow F^1A'$	16a″ → 20a″	0.50	4.37 (284)	0.3157	ILCT
		2			
$X^1A' \rightarrow A^1A'$	17a″ → 18a″	0.67	2.47 (501)	0.1646	MLCT/LLCT
$X^1A'' \rightarrow B^1A''$	79a′ → 18a″	0.70	3.05 (406)	0.0043	MLCT
$X^1A' \rightarrow C^1A'$	17a″ → 19a″	0.69	3.07 (404)	0.0545	MLCT/LLCT
$X^1A' \rightarrow D^1A'$	16a″ → 19a″	0.63	3.36 (369)	0.1878	MLCT/ILCT
$X^1A' \rightarrow E^1A'$	15a″ → 18a″	0.56	3.54 (350)	0.0900	MLCT/LLCT
$X^1A' \rightarrow F^1A'$	15a″ → 19a″	0.65	4.20 (295)	0.1947	MLCT/ILCT
$X^1A' \rightarrow G^1A'$	17a″ → 21a″	0.55	4.44 (280)	0.4471	ILCT
		3			
$X^1A' \rightarrow A^1A'$	16a″ → 17a″	0.68	2.49 (498)	0.1585	MLCT/LLCT
$X^1A'' \rightarrow B^1A''$	76a′ → 17a″	0.70	3.07 (404)	0.0042	MLCT
$X^1A' \rightarrow C^1A'$	16a″ → 18a″	0.69	3.18 (390)	0.0490	MLCT/LLCT
$X^1A' \rightarrow D^1A'$	15a″ → 18a″	0.63	3.36 (369)	0.1909	MLCT/ILCT
$X^1A' \rightarrow E^1A'$	15a″ → 17a″	0.44	3.76 (330)	0.2284	MLCT/LLCT
$X^1A' \rightarrow F^1A'$	14a″ → 18a″	0.42	4.44 (279)	0.1224	MLCT/ILCT
$X^1A' \rightarrow G^1A'$	16a″ → 20a″	0.43	4.47 (277)	0.4552	ILCT

compare the absorptions in media with different polarities, the absorptions for **1**−**3** in CH_3CN solution were also calculated, and the results are listed in Table S2 (Supporting Information). Table S2 shows that, when the solvent is changed from CH_2Cl_2 to CH_3CN, the character of absorptions is completely unchanged, but the low-lying MLCT/LLCT absorptions in **1**−**3** are progressively blue-shifted by ca. 0.1 eV in energy, and an inconspicuous shift (<0.04 eV) is observed for the higher-lying ILCT absorptions. The blue shift in the low-lying absorptions is correlated with a weak negative solvatochromic effect in the experiments. McMillin et al.[5b] suggested that, for 4′-substituted aryl terpyridyl platinum(II) chlorine complexes, CT bands showing ILCT and MLCT character in absorption can exhibit a solvent dependence. Our calculations are in agreement with the experimental observations and conclusions reported in the literature.

It is well-known that TD-DFT calculations that do not consider solvent effects cannot form the basis of a reasonable analysis of experimental spectra. Therefore, we show the MO energy levels of **3** in gas and solution as an example to compare the effect of a solvent on the absorptions. It can be seen in Figure 4 that the HOMOs are stabilized, but the LUMOs are more destabilized in solution, and hence, the HOMO−LUMO energy gap is dramatically increased (∼0.6 eV) in solution relative to that in the gas phase. Furthermore, the HOMO−LUMO gap in CH_2Cl_2 and CH_3CN solution is 0.1 eV, which is comparable to the difference in low-lying absorption energy in the two solutions and further indicates that the low-lying absorptions mainly come from the excitation of the HOMO → LUMO transition.

3.4. Emission Spectra. According to TD-DFT calculations, the lowest-energy emissions for **1**−**3** were obtained at 623, 657, and 681 nm, respectively, in CH_2Cl_2 solution (see Table 4), which correspond to the respective experimental values of 582, 615, and 640 nm.[9]

To conveniently discuss the nature of the emission, we present the compositions of the frontier MOs of **1**−**3** related to the emission in CH_2Cl_2 solution in Table 5. For **1**, the calculated lowest-energy emission occurs at 623 nm in solution with the nature of a $^3A' \rightarrow {}^1A'$ transition. In the transition, the triplet excited-state configuration of 16a″ (HOMO) → 17a″ (LUMO) with the maximum CI coefficient of 0.7 mostly contributes to the transition. As seen in Table 5, the HOMO (16a″) is composed of about 28% Pt(II) d_{yz} atomic orbital and 64% C≡CPh ligand, whereas the LUMO (17a″) is mainly (85%) localized on the bipyridine fragment. Thus, the emission at 623 nm for **1** is assigned to the combined transitions of ^{3}MLCT and ^{3}LLCT [C≡CPh/Pt(II) → bipyridine]. For **2** and **3**, the

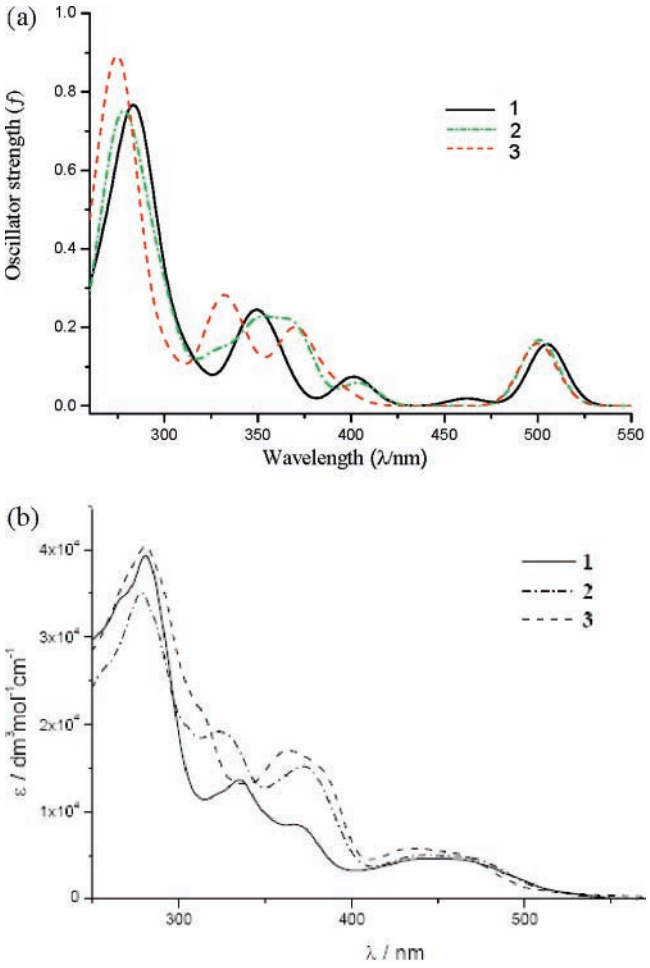

Figure 3. Simulated absorption spectra of **1**−**3** in CH_2Cl_2 solution compared to the experimental spectra: (a) calculated absorption spectra, (b) experimental absorption spectra obtained from ref 9.

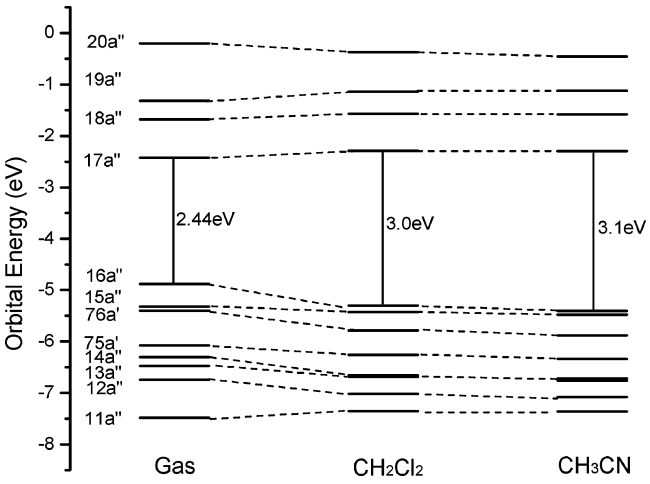

Figure 4. Comparison of energy levels of **3** in the gas phase, CH_3CN solution, and CH_2Cl_2 solution.

HOMO → LUMO transition is also the leading configuration in the $^3A' \rightarrow {}^1A'$ transition of the emissions. As seen in Table 5, the LUMO (18a″) of **2**, similar to that of **1**, has ca. 89% π^* orbital localized on bipyridine, whereas the initial orbital of **2** is different from that of **1**, as the HOMO (17a″) is composed of 28% Pt d_{xz} and 71% N^N^S π orbital. Therefore, the emission at 657 nm of **2** has a ^{3}ILCT transition character localized on the tridentate ligand and perturbed by ^{3}MLCT transition coming from the metal Pt(II) to bipyridine. Analogous to **2**, the lowest-lying $^3A'$ excited state gives rise to the emission at 681 nm for **3**, comparable to the measured phosphorescence at 640 nm in the experiments. The case for **3** is similar to that for **2**, so the luminescence of **3** is also assigned to a mixed ^{3}MLCT and ^{3}ILCT transition. In addition, it is worth noting that the calculated phosphorescence maxima for **1**−**3** are all red-shifted by ca. 0.12−0.14 eV relative to the corresponding experimental values. The minor discrepancy can be attributed to the poor asymptotic behavior of the exchange-correlation potential of the TD-DFT method. To intuitively understand the nature of the emission, diagrams of the single-electron transitions related to the phosphorescence of **1**−**3** are shown in Figures 5−7, respectively.

The emission energies for **1**−**3** are in the order **1** > **2** > **3**, which is consistent with the experimental results. From the above analysis, we know that the nature of the emission of **1** is attributed to a mixed ^{3}LLCT and ^{3}MLCT transitions, whereas those of **2** and **3** are assigned as combined ^{3}ILCT and ^{3}MLCT transitions. It is well known that the transition energy of the ^{3}LLCT state is higher than that of the ^{3}ILCT state, so it is not surprising that the emission energy of **1** is higher than those of **2** and **3**. However, the energy order between **2** and **3** is slightly complicated and can be explained from the following two points: (1) In contrast to **1**, in which only the LUMO has π^* orbital character, both the HOMOs and LUMOs for **2** and **3** are all localized on the π^*-based cyclometalated ligands. Therefore, the HOMOs and LUMOs for **2** and **3** are simultaneously stabilized by the extended π orbital. (2) On the other hand, because the polarizability and basicity are higher for S

TABLE 4: Phosphorescent Emissions of 1−3 in CH_2Cl_2 Solution According to TD-DFT (B3LYP) Calculations and Associated Experimental Values

	transition	configuration	coeff	*E* (nm) (eV)	assignment	exp[a] (nm)
1	$^3A' \rightarrow {}^1A'$	16a″ → 17a″	0.70	623 (1.99)	MLCT/LLCT	582
2	$^3A' \rightarrow {}^1A'$	16a″ → 18a″	0.71	657 (1.89)	MLCT/ILCT	615
3	$^3A' \rightarrow {}^1A'$	16a″ → 17a″	0.70	681 (1.82)	MLCT/ILCT	640

[a] Reference 9.

TABLE 5: Compositions of Partial Frontier MOs of 1−3 in CH_2Cl_2 Solution in the Lowest-Lying $^3A'$ Excited State

1

			N^N^C		
MO	*E* (eV)	Pt	bipyridine	phenyl	C≡CPh
20a″	−0.7456	8.1p + 3d_{yz}	12.1	4.5	71.0
18a″	−1.7799	1.7p + 1.0d_{xz}	71.4	23.6	2.2
17a″[a]	−2.5963	3.5p + 3.1d_{yz}	85.6	3.6	4.2
16a″[b]	−5.4140	27.9d_{yz}	6.2	1.0	63.8
12a″	−7.1904	32.2d_{yz}	40.2	2.9	24.5

2

			N^N^S		
MO	*E* (eV)	Pt	bipyridine	thienyl	C≡CPh
19a″	−1.8509	2.3p + 2.6d_{yz}	62.2	31.1	1.8
18a″[a]	−2.6148	3.9p + 2.7d_{yz}	83.5	6.4	3.5
17a″[c]	−5.5916	26.5d_{xz}	24.1	48.2	0.9

3

			N^N^O		
MO	*E* (eV)	Pt	bipyridine	furyl	C≡CPh
18a″	−1.7307	2.5p + 2.2d_{xz}	69.4	23.4	2.4
17a″[a]	−2.6172	3.8p + 3.1d_{yz}	85.4	4.0	3.6
16a″[b]	−5.5220	24.5d_{xz}	23.9	41.3	9.7
15a″	−5.5933	24.4d_{yz}	10.0	11.0	54.0

[a] LUMO. [b] HOMO.

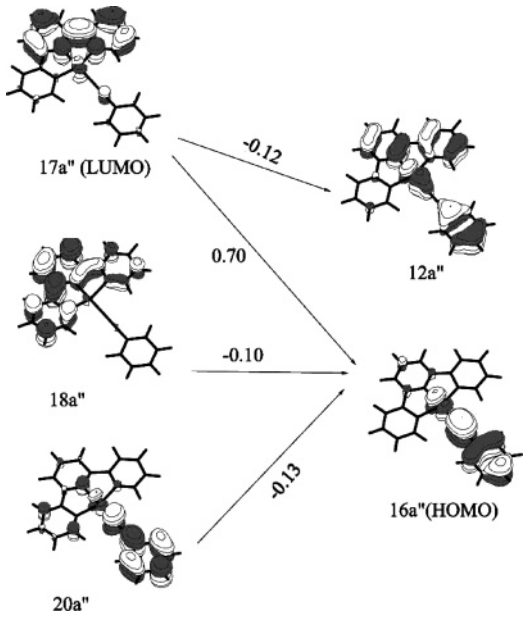

Figure 5. Single-electron transitions with |CI coefficients| > 0.1 according to TD-DFT calculations for the 623-nm emission of [Pt(N^N^C)C≡CPh]$^+$ (**1**) in dichloromethane.

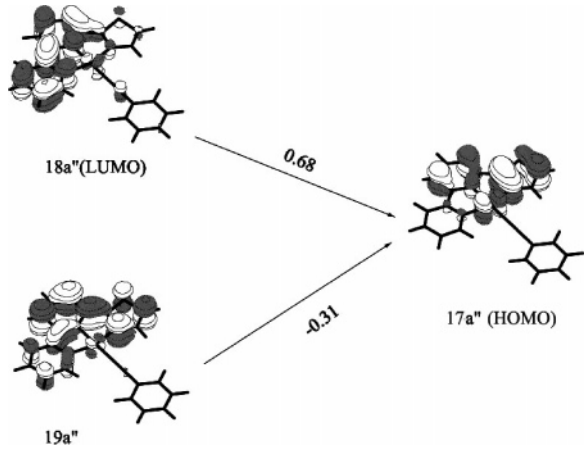

Figure 6. Single-electron transitions with |CI coefficients| > 0.1 according to TD-DFT calculations for the 657-nm emission of [Pt(N^N^S)C≡CPh]$^+$ (**2**) in dichloromethane.

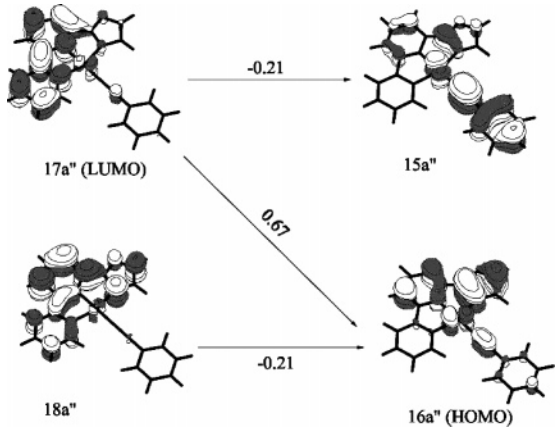

Figure 7. Single-electron transitions with |CI coefficients| > 0.1 according to TD-DFT calculations for the 681-nm emission of [Pt(N^N^O)C≡CPh]$^+$ (**3**) in dichloromethane.

than O, the ligand-field strength is in the order thienyl > furyl. Therefore, if we assume that the HOMOs have the identical orbital energy levels for **2** and **3**, then the LUMO energy is further destabilized by thienyl. Therefore, these two points result in the HOMO−LUMO gap being higher for **2** (2.977 eV) than for **3** (2.905 eV); hence, the emission energy of **3** is red-shifted relative to that of **2**.

TABLE 6: Dipole Moments (μ), Polarizabilities (α), and Static First Hyperpolarizabilities (β_0) of 1−3 and the Corresponding N^N^A Ligands

	μ (au)	α (au)	β_0 (au)
1	3.553	374	7126
N^N^C	1.012	184	175
2	3.294	368	6733
N^N^S	0.856	181	303
3	3.226	350	6649
N^N^O	0.850	167	531

3.5. NLO Properties. The NLO response is one of the most important physical characteristics of optical materials. Here, we predict that **1**−**3** might be potential candidates as novel NLO materials. Three reasons support our prediction: (1) All three complexes have a planar geometry with a positive dipole moment, which is one of the most critical factors in having a nonzero static first hyperpolarizability (β_0). (2) The complexes show distinct CT excited states, which can produce electrons and holes and make it possible for the electrons and holes to interact. (3) The NLO response can be greatly enhanced by π delocalization on the polypyridyl and phenylacetylide fragments.

In Table 6, we list the dipole moments (μ), polarizabilities (α), and static first hyperpolarizabilities (β_0) of **1**−**3**. From Table 6, one can see that the dipole moments of **1**−**3** are 3.553, 3.293, and 3.226 au and the polarizabilities of the complexes are 374, 368, and 350 au, respectively. The values of μ and α of **1**−**3** are very close and small. The static first hyperpolarizabilities of **1**−**3** are 7126, 6733, and 6649 au, respectively, which are almost 20 times larger than μ and α. Because the static first hyperpolarizability can represent an NLO response character, the NLO activities of the complexes are in the order **1** > **2** > **3**, in accordance with the aromaticity order of the cyclometalated ligands.

To highlight the function of the platinum(II) ion in the NLO response, we also optimized the geometries of the N^N^C, N^N^S, and N^N^C ligands at the same theoretical level as used for **1**−**3** and calculated the corresponding μ, α, and β_0 values in the respective N^N^C, N^N^S, and N^N^O ligands, as listed in Table 6. The optimization was carried out without symmetry constraints, and C_1 symmetry was adopted by the isolated cyclometalated ligands. The results show that the cyclometalated ligands still retain a planar geometry, indicated by the ca. 0° dihedral angles between the substituent aryl and pyridyl rings. Because the distances between the lateral nitrogen and carbon are 4.527, 4.710, and 4.862 Å in the N^N^C, N^N^S, and N^N^O ligands, respectively, which is elongated by about 11−20% compared to those in **1**−**3**, it is conceived that there is no repulsion in the respective rings in the N^N^C, N^N^S, and N^N^O ligands. This is unlike the case in the terpyridine ligand,[10a] in which the two lateral pyridine rings are twisted by ca. 30° with respect to the central ring in order to minimize the repulsion between the three nitrogen lone pairs. We note that the μ, α, and β_0 values of the cyclometalated ligands are very small; in particular, the values of β_0 are almost 10−40 times smaller than those of **1**−**3**. The considerable shift in β_0 can be rationalized in terms of the interaction of the metal Pt(II) with the cyclometalated ligand, which can dramatically influence the NLO response character by the MLCT and LLCT excited states. Our results agree well with the conclusions by Tessore et al.,[10] who elucidated that the importance of the metal in the enhanced NLO response, and the shifts in NLO response upon the

coordination of metal to trpy ligand are controlled by the CT transitions, such as MLCT and LLCT transitions.

4. Conclusions

To provide insight into the properties of their ground and excited states, detailed calculations of **1**−**3** were performed at the DFT level. The completed absorption spectra and the lowest-energy emissions for the three complexes in the UV/vis region were predicted by the TD-DFT approach combined with the PCM solvent model.

The calculations reveal that the lowest-lying absorptions for **1**−**3** are all derived from the combined LLCT and MLCT transitions. Their absorption energies are very close; only that of **1** is slightly red-shifted relative to those of **2** and **3**. The red shift comes from the different electronic structures and the polarizability and basicity of phenyl, thientyl, and furyl ligands. With increasing solvent polarity (from CH_2Cl_2 to CH_3CN), the lowest-lying LLCT/MLCT absorptions are red-shifted by ca. 0.1 eV, but the energies of the ILCT absorptions basically do not undergo any change. This is comparable to the negative solvatochromism effect observed experimentally.

The optimized geometric parameters of **1**−**3** in the ground state are in agreement with the experimentally measured values. The three substituent aryl rings (phenyl, thientyl, and furyl) do not have an impact on the geometry in the ground state. However, upon excitation, the variation of the bond lengths, such as those of Pt−C and C≡C, shows some contrary trends relative to the ground state, which corresponds to the different natures of the lowest-energy emissions for the three complexes. The nature of the lowest-energy emission of **1**, similar to the lowest-lying absorption, is assigned to the combination of ^{3}LLCT and ^{3}MLCT transitions. In contrast to **1**, the lowest-energy emissions for **2** and **3** come from the ^{3}ILCT transition perturbed by some ^{3}MLCT transition. The emission wavelengths are in the order **1** < **2** < **3**, and the red shift of the wavelength can be viewed as the differences in the natures of the transitions and electronic structures for the substituent aryl rings.

Finally, we explored the NLO response characteristics for **1**−**3** at the DFT level and found that the nonzero static first hyperpolarizability (β_0) values for **1**−**3** increased by almost 10−40 times through the introduction of metal Pt(II) into the cyclometalated ligands. MLCT and LLCT transitions are responsible for the large discrepancy.

Acknowledgment. This work was supported by the Natural Science Foundation of China (Nos. 20573042, 20333050, 20173021), the Natural Science Foundation of Heilongjiang Province of China (No. B200601), and the Science Foundation for Excellent Youth of Heilongjiang University of China (No. JC2006L2)

Supporting Information Available: Tables for the dissected NICS values of the N^N^C, N^N^S, and N^N^O ligands, absorption data in CH_3CN solution, and the plot of NICS values at 0.0−2.0 Å above the ring center of the phenyl, thienyl, and furyl ligands. This material is available free of charge via the Internet at http://pubs.acs.org.

References and Notes

(1) (a) Miskowski, V. M.; Houlding, V. H. *Inorg. Chem.* **1991**, *30*, 4446. (b) Miskowski, V. M.; Houlding, V. H. *Inorg. Chem.* **1989**, *28*, 1529. (c) van Slageren, J.; Klein, A.; Záliš, S. *Coord. Chem. Rev.* **2002**, *230*, 193. (d) Klein, A.; van Slageren, J.; Záliš, S. *J. Organomet. Chem.* **2001**, *620*, 202. (e) Klein, A.; van Slageren, J.; Záliš, S. *Eur. J. Inorg. Chem.* **2003**, 1927. (f) Lai, S. W.; Chan, M. C. W.; Cheung, K. K.; Che, C. M. *Organometallics* **1999**, *18*, 3327. (g) Guo, F. Q.; Sun, W. F.; Liu, Y.; Schanze, K. *Inorg. Chem.* **2005**, *44*, 4055. (h). Deinis, K. C. T.; McMillin, D. R. *Coord. Chem. Rev.* **2001**, *211*, 195. (i) Büchner, R.; Field, J. S.; Haines, R. J.; Cunningham, C. T.; McMillin, D. R. *Inorg. Chem.* **1997**, *36*, 3952. (j) Yip, H. K.; Cheng, L. K.; Cheung, K. K.; Che, C. M. *J. Chem. Soc., Dalton Trans.* **1993**, 2993.

(2) (a) McGarrach, J. E.; Kim, Y. J.; Hissler, M.; Eisenberg, R. *Inorg. Chem.* **2001**, *40*, 4510. (b) Wadas, T. J.; Wang, Q. M.; Kim, Y. J.; Flaschenreim, C.; Blanton, T. N.; Eisenberg, R. *J. Am. Chem. Soc.* **2004**, *126*, 16841. (c) Hissler, M.; Connick, W. B.; Geiger, D. K.; McGarrah, J. E.; Donald, Lipa.; Lachicotte, R. J.; Eisenberg, R. *Inorg. Chem.* **2000**, *39*, 447.

(3) (a) Kunkely, H.; Vogler, A. *J. Am. Chem. Soc.* **1990**, *112*, 5625. (b) Wan, K. T.; Che, C. M.; Cho, K. C. *J. Chem. Soc., Dalton Trans.* **1991**, 1077. (c) Maestri, M.; Sandrini, D.; von Zelewsky, A.; Deuschel-Cornioley, C. *Inorg. Chem.* **1991**, *30*, 2476.

(4) (a) Wong, E.; Giandomenico, C. M. *Chem. Rev.* **1999**, *99*, 2451. (b) Arena, G.; Scolaro, L. M.; Pasternack, R. F.; Romeo, R. *Inorg. Chem.* **1995**, *34*, 2994. (c) Peyratout, C. S.; Aldridge, T. K.; Crites, D. K.; McMillin, D. R. *Inorg. Chem.* **1995**, *34*, 4484. (d) Cusumano, M.; Di Pietro, M. L.; Giannetto, A. *Inorg. Chem.* **1999**, *38*, 1754.

(5) (a) Aldridge, T. K.; Elizabeth, M. S.; McMillin, D. R. *Inorg. Chem.* **1994**, *33*, 722. (b) Michalec, J. F.; Bejune, S. A.; Cuttell, D. G.; Summerton, G. C.; Gertenbach, J. A.; John, S. F.; Raymond, J. H.; McMillin, D. R. *Inorg. Chem.* **2001**, *40*, 2193.

(6) (a) Yam, V. W. W.; Tang, R. P. L.; Wong, K. M. C.; Cheung, K. K. *Organometallics* **2001**, *20*, 4476. (b) Yang, Q. Z.; Wu, L. Z.; Wu, Z. X.; Zhang, L. P.; Tung, C. H. *Inorg. Chem.* **2002**, *41*, 5653. (c) Guo, F. Q.; Sun, W. F.; Liu, Y.; Schanze, K. *Inorg Chem.* **2005**, *44*, 4055.

(7) (a) Büchner, R.; Cunningham, C. T.; Field, J. S.; Haines, R. J.; McMillin, D. R.; Summerton, G. C. *J. Chem. Soc., Dalton Trans.* 1999, 711. (b) Michalec, J. F.; Bejune, S. A.; McMillin, D. R. *Inorg. Chem.* **2000**, *39*, 2708. (c) Crites, D. K.; Cunningham, C. T.; McMillin, D. R. *Inorg. Chem. Acta* **1998**, *273*, 346. (d) Yip, H. K.; Cheng, L. K.; cheung, K. K.; Che, C. M. *J. Chem. Soc., Dalton Trans*. **1993**, 2933.

(8) (a) Lu, W.; Mi, B. X.; Chan, M. C. W.; Hui, Z.; Zhu, N. Y.; Lee. S. T.; Che. C. M. *Chem. Commun.* **2002**, 206. (b) Che. C. M.; Fu, W. F.; Lai, S. W.; Hou, Y. J.; Liu, Y. L. *Chem. Commun.* **2003**, 118. (c) Williams, J. A. G.; Beeby, A.; Davies, E. S.; Weinstein, J. A.; Wilson, C. *Inorg. Chem.* **2003**, *42*, 8609. (d) Farley, S. J.; Rochester, D. L.; Thompson, A. L.; Howard, J. A. K.; Willams, J. A. G. *Inorg. Chem*. **2005**, *44*, 9690. (e) Constable, E. C.; Henney, R. P. G.; Leese, T. A.; Tocher, D. A. *J. Chem. Soc., Chem. Commun*. **1990**, 513.

(9) Lu. W.; Mi, B. X.; Chan, C. W.; Hui, Z.; Che, C. M.; Zhu, N. Y.; Lee, S. T. *J. Am. Chem. Soc.* **2004**, *126*, 4958.

(10) (a) Tessore, F.; Roberto, D.; Ugo, R.; Pizzotti, M.; Quici, S.; Cavazzini, M.; Bruni, S.; De Angelis, F. *Inorg. Chem*. **2005**, *44*, 8967. (b) De Angelis, F.; Fantacci, S.; Sgamelotti, A; Cariati, F.; Roberto, D.; Tessore, F.; Ugo, R. *Dalton. Trans*. **2006**, 852.

(11) (a) Becke, A. D. *J. Chem. Phys.* **1993**, *98*, 5468. (b) Stevens, P. J.; Devlin, J. F.; Chabalowski, C. F.; Frisch, M. J. *J. Phys. Chem.* **1994**, *98*, 11623. (c) Becke, A. D. *Phys. Rev. A* **1988**, *38*, 3098. (d) Lee, C.; Wang, W.; Parr, R. G. *Phys. Rev. B* **1988**, *37*, 785.

(12) (a) Casida, M. E.; Jamorski, C.; Casida, K. C.; Salahub, D. R. *J. Chem. Phys.* **1998**, *108*, 4439. (b) Stratmann, R. E.; Scuseria, G. E. *J. Chem. Phys.* **1998**, *109*, 8218. (c) Matsuzawa, N. N.; Ishitani, A. *J. Phys. Chem. A* **2001**, *105*, 4953.

(13) (a) Cossi, M.; Scalmani, G.; Regar, N.; Barone, V. *J. Chem. Phys.* **2002**, *117*, 43. (b) Barone, V.; Cossi, M. *J. Chem. Phys.* **1997**, *107*, 3210.

(14) (a) Schleyer, P. v. R.; Manoharan, M.; Wang, Z. X.; Kiran, B.; Jiao, H. J.; Puchta, R.; Hommes, N. J. R. v. E. *Org. Lett.* **2001**, *3*, 2465. (b) Corminboeuf, C.; Heine, T.; Seifert, G.; Schleyer, P. v. R.; Weber, J. *Phys. Chem. Chem. Phys.* **2004**, *6*, 273. (c) Cyranski, M. K.; Krygowski, T. M.; Katritzky, A. R.; Schleyer, P. v. R. *J. Org. Chem.* **2002**, *67*, 1333.

(15) (a) McLean, A. D.; Yoshimine, M. *J. Chem. Phys*. **1967**, *47*, 1927. (b) Li, Y.; Li, Z. R.; Wu, D.; Li, R. Y.; Hao, X. Y.; Sun, C. C. *J. Phys. Chem. A* **2004**, *108*, 3145.

(16) Frisch, M. J.; Trucks, G. W.; Schlegel, H. B.; Scuseria, G. E.; Robb, M. A.; Cheeseman, J. R.; Montgomery, J. A., Jr.; Vreven, T.; Kudin, K. N.; Burant, J. C.; Millam, J. M.; Iyengar, S. S.; Tomasi, J.; Barone, V.; Mennucci, B.; Cossi, M.; Scalmani, G.; Rega, N.; Petersson, G. A.; Nakatsuji, H.; Hada, M.; Ehara, M.; Toyota, K.; Fukuda, R.; Hasegawa, J.; Ishida, M.; Nakajima, T.; Honda, Y.; Kitao, O.; Nakai, H.; Klene, M.; Li, X.; Knox, J. E.; Hratchian, H. P.; Cross, J. B.; Adamo, C.; Jaramillo, J.; Gomperts, R.; Stratmann, R. E.; Yazyev, O.; Austin, A. J.; Cammi, R.; Pomelli, C.; Ochterski, J. W.; Ayala, P. Y.; Morokuma, K.; Voth, G. A.; Salvador, P.; Dannenberg, J. J.; Zakrzewski, V. G.; Dapprich, S.; Daniels, A. D.; Strain, M. C.; Farkas, O.; Malick, D. K.; Rabuck, A. D.; Raghavachari, K.; Foresman, J. B.; Ortiz, J. V.; Cui, Q.; Baboul, A. G.; Clifford, S.; Cioslowski, J.; Stefanov, B. B.; Liu, G.; Liashenko, A.; Piskorz, P.; Komaromi, I.; Martin, R. L.; Fox, D. J.; Keith, T.; Al-Laham, M. A.; Peng, C. Y.; Nanayakkara, A.; Challacombe, M.; Gill, P. M. W.; Johnson, B.; Chen, W.; Wong, M. W.; Gonzalez, C.; Pople, J. A. *Gaussian 03*, revision B.03; Gaussian, Inc.: Pittsburgh, PA, 2003.

(17) Pyykkö, P.; Mendizabal, F. *Inorg. Chem.* **1998**, *37*, 3018.

(18) Pan, Q. J.; Zhang, H. X. *Chem. Phys. Lett.* **2004**, *394*, 155.